A NEW ACTIVE CLAMP CURRENT- FED FULL-BRIDGE DC–DC CONVERTER FOR HIGH-VOLTAGE APPLICATIONS

V.Delbin Jelaja
Research Scholar, Department of Electrical Engineering, Anna University, Chennai, India,
djelaja@yahoo.com

M.Rajaram
Vice Chancellor, Anna University, Chennai, India,
rajaramgct@rediffmail.com

Abstract: *In this article, a new soft switching full-bridge DC–DC converter with phase shift control is proposed to reduce the circulating loss on the primary side and the voltage stress on the secondary side of the transformer. The conventional converter has the drawbacks such as circulating loss in the primary and voltage spike across the rectifier diode. Also, the conventional system uses a large output inductor in the secondary side; because of these properties, core loss occurs. The proposed technique overcome the above-mentioned drawbacks, by which without an auxiliary circuit, a single common active clamp branch is employed for zero-voltage-switching in all active switches, which reduces the circulating loss on the primary side and switching losses. To introduce the converter without an additional inductor, the transformer leakage inductance is utilized as the resonant inductor. The resonance between the transformer leakage inductance and the rectifier capacitor can reduce the current stresses of the rectifier diodes and the conduction losses. The proposed converter has many advantages including high efficiency, low cost, and minimum number of devices. This converter is conducive for high-voltage and high-power applications. Experimental analysis of the proposed converter shows better performance than other converter dealt with the literature.*

Keywords: *DC–DC converters, phase-shifted full-bridge converter (PSFB), pulse-width modulation converters, soft switching, zero current switching, zero voltage switching.*

1. INTRODUCTION

In general, the control over output power, torque, and the speed of DC motors is applied through power electronic converters. These converters affect both the power factor and the power efficiency. If the switching frequency of the converter is low, the power efficiency is high whereas the power factor of the converter is remarkably low. In this case, because the order of main harmonics is low, we need a large passive filter. To design a low-cost and low-weight converter, high-frequency operation is necessary. The choice of high switching frequency reduces the dimension of the filter and the size of magnetic elements, increases the power factor, and reduces other reactive components used in the converters. The choice of a power level higher than 500 W is better suited for the phase-shifted full-bridge (PSFB) DC–DC converter. This will ensure a higher level of efficiency and low electromagnetic interference. But the circulating loss in the primary is high for a conventional PSFB converter, especially in a high input current application. The second limitation of the traditional PSFB converter is high voltage overshoot and oscillation across the output rectifier diodes when they are turned OFF. The zero-voltage and zero-current switching (ZVZCS) technique is proposed, based on the PSFB converter, to reduce the circulating loss. The key point of this technique is the use of a transformer leakage inductor as a resonant inductor, which helps in achieving ZVZCS in the entire operating range.

a) The zero-voltage-switching (ZVS) range can be extended by adding an external series inductor [1]. However, a series inductance can extend the time required for the primary current to change direction from the negative to the positive or vice

versa, which results in a loss of effective duty cycle on the secondary side of the transformer and decreases the conversion efficiency. Normally, a transformer with high turns ratio is required to overcome the effective duty-cycle loss. But high turns ratio increases the reflected output current into the primary side, which results in high primary circulating loss. In addition, high turns ratio increases the voltage stress on the secondary-side bridge rectifier. Instead of external series inductance, the inductive energy stored in the additional auxiliary circuit has been proposed [2, 3]. The proposed method has a high power loss for wide load range operations. A resistor–capacitor–diode snubber circuit was introduced in reference [4]. The main problem with the snubber circuit for high-power applications is that the amount of loss in the snubber resister is high, which degrades the efficiency of the converter. In references [5]–[8], active clamp zero-voltage transition (ZVT) is realized. It is necessary to use two main switches. Zero-current transition (ZCT) is not implemented. To obtain an active clamp, two auxiliary switches are used. In addition, the converter requires a special design transformer and two rectifier diodes. In references [9]- [14] the main switch turns ON with ZVT and turns OFF with ZCT. There are no additional voltage and current stresses in the main switch and the main diode. A magnetic-coupled inductance is used in the circuit. If the magnetic coupling is not good, high voltage spikes and losses occur due to the transformer leakage inductance. In references [15] and [16], the low-side and high-side switches are operated with hard switching turn-off condition, which results in high-voltage spikes. In references [17] and [18], an LLC series resonant converter (SRC) is designed within the above resonance region; its operation is the same as that of SRC and hence the drawbacks of the SRC are found in the LLC SRC. The drawback of the SRC is that ZVS operation cannot be achieved under the light-load condition. To raise the power level, a dual full-bridge configuration is adopted, and the same is indicated in reference [19]. Owing to the transfer of power during period of freewheeling, the size of output filter is reduced and the efficiency is improved in the converters proposed in references [20]–[25]. But at the same time it has the circulating current problem too. High-frequency transformer-isolated DC–DC converter [26–28] translates the low fuel cell stack voltage to higher than the peak of the utility line or inverter output voltage specification with necessary isolation. It reduces the thermal stress on the components, electromagnetic interference and switching losses, and improves the efficiency. It occurs particularly at light load where the switching and conduction losses are comparable or switching losses dominate the conduction losses. As non-isolated DC–DC converters are common and low cost, they are used in most negative ground application in vehicles for various DC-powered appliances. But, there is a disadvantage in having the electrical connection between the input and the output: it offers no protection to the load against any high electrical voltage, high electrical current that occurs on the input side. They also have less noise-filtering capability. A non-isolated bidirectional converter with active clamping has been proposed in reference [29] for ZVS up to 40% load, but operation with wide input voltage variation is not reported here. A solution to achieve ZVS over 1:2 source voltage variation using several extra components is given in reference [30] without discussing ZVS for variation in load. In references [31]–[33], switch parallel capacitors are used and are reported to be working.

This article proposes a PSFB converter without circulating loss in the primary side. Furthermore, the voltage stress and current stress of the rectifier diode are reduced to a much lower value compared with those in the previous ZVZCS converter. The circuit diagram is shown in Fig 1. It consists of four main switches and one auxiliary clamp switch, which performs ZVS through the use of resonance between transformer leakage inductance (L_k) and the rectifier capacitors, which can reduce the current stress of the rectifier diodes and conduction losses. The clamping diode is used to clamp the voltage spike across the rectifier diode. The DC–DC converter is pulse-width modulation (PWM) controlled, so implementation of control circuit is very simple and inexpensive. Because this converter has just one input boost inductor and it does not use any clamp windings, its cost and size can be further reduced in comparison with previous converters. The operating principles and theoretical analysis of the proposed converter are verified.

2. PROPOSED DC–DC CONVERTER DESCRIPTION AND OPERATION

The circuit diagram and key waveforms of the proposed converter are shown in Figs. 1 and 2, respectively. The proposed converter consists of a single active clamp branch, a PSFB, a single-phase

transformer, and a voltage-doubler circuit, which are all connected to a DC motor load. The single active clamp branch is responsible for soft switching in all active switches. The magnetizing current of transformer is negligible.

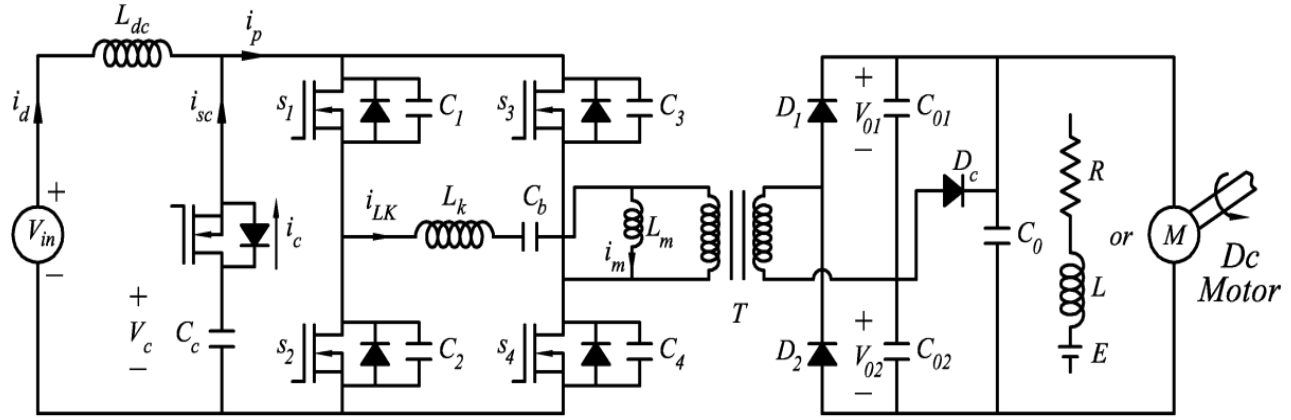

Fig. 1. Circuit diagram of the proposed converter

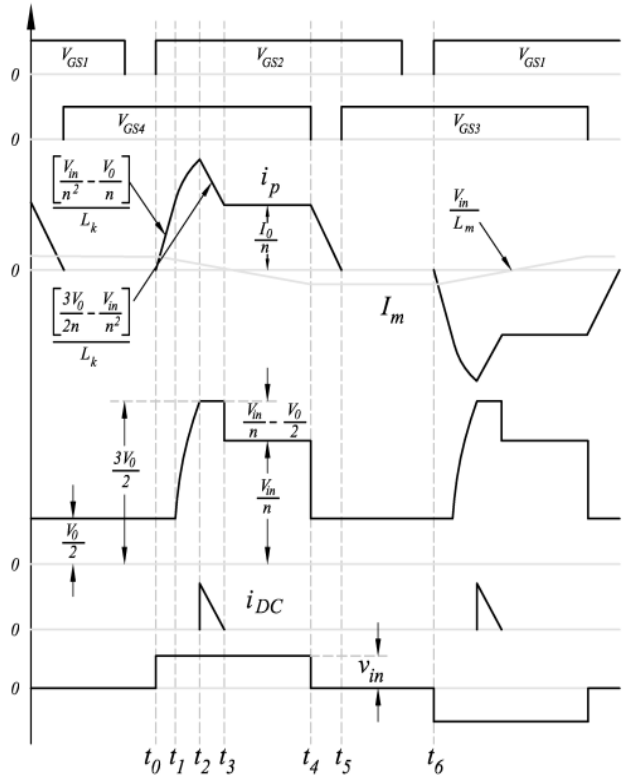

Fig. 2. Key waveforms in one switching cycle

2.1Mode 1 (t_0–t_1)

At t_0, S_4 turns on the voltage across the input side, which reaches the clamp capacitor voltage V_c and the clamp diode. The latter is the body diode of MOSFET S_c, which conducts the boost inductor current (i_d). The current through the leakage inductance (i_{LK}) increases is determined by the voltage difference between the clamp voltage (V_c) and the reflected output voltage (V_0). To facilitate ZVS, the clamp switch (S_c) is turned on before the clamp current (i_c) reverses at t_1. It should be observed that i_c is $-i_d$ at t_0. Apply KCL,

$$i_c = -(i_d - i_{Lk}) \quad \text{.....} \quad (1)$$

The primary side current (i_p) increases linearly until it reaches the current reflected from the output side as follows:

$$i_p(t) = \frac{1}{n}[\frac{V_{in}}{n} - V_{01}(t_0)]\frac{1}{z_0}\sin\omega_r(t-t_0) + i_m(t-t_0) \text{.....} \quad (2)$$

where

$$\omega_r = \frac{n}{\sqrt{L_k C_r}},\ Z_0 = \frac{1}{n}\sqrt{\frac{L_k}{C_r}},\ C_r = C_{01} + C_{02}$$

The magnetizing current, which also increases with the resonance between the magnetizing inductor and the rectifier capacitors, is obtained as follows:

$$i_m(t) = i_m(t_0)\cos\omega_m(t-t_0) + \frac{nV_{01}(t_0)}{Z_m}\sin\omega_m(t-t_0) \text{.....} \quad (3)$$

where $\omega_m = \frac{n}{\sqrt{L_m C_r}},\ Z_m = n\sqrt{\frac{L_m}{C_r}}$

Because the resonant frequency $\left(f_m = \frac{\omega_m}{2\pi}\right)$ is much slower than the switching frequency, the magnetizing current can linearly be approximated as follows:

$$i_m(t) = i_m(t_0) + \frac{nV_{01}(t-t_0)}{L_m}(t-t_0) \text{ .....} \quad (4)$$

2.2 Mode 2 (t_1–t_2)

When switch s_1 is turned off at t_1, mode 2 begins; the primary current i_p starts to charge and discharge the output capacitors of switches s_1 and s_2, respectively. The voltage across the primary side decreases. But still diode D_1 is conducting, and the voltage across the magnetizing inductance is maintained to be nV_{01}

The clamp current (i_c) provides the difference between increasing primary current and constant boost inductor current

$$i_{c(max)} = -(i_d - i_{Lk(max)}) \quad \text{..... (5)}$$

At t_1, the transformer leakage inductance is resonant with the rectifier capacitors of the converter. The magnitude of resonant voltage and current can be calculated as follows:

$$i_{LK}(t) = I_0 + \frac{\frac{V_{in}}{n} - V_{01}}{Z_r} \sin \omega_r (t - t_1) \quad \text{..... (6)}$$

$$V_c(t) = \frac{V_{in}}{n}(1 - \cos \omega_r (t - t_1)) + V_{01} \cos \omega_r (t - t_1) \quad \text{.....(7)}$$

Where $V_c(t)$ is the resonant capacitor voltage. This interval ends when the voltage across the voltage doubler increases to $3V_0/2$.

Where, $Z_r = \frac{1}{n}\sqrt{\frac{L_k}{C_r}}$, $C_r = C_{01} + C_{02}$, $\omega_r = \frac{n}{\sqrt{L_k C_r}}$,

2.3 Mode 3(t_2–t_3)

At t_3, the voltage across the rectifier increases and it reaches $3\frac{V_0}{2}$ when the clamping diode D_c begins to conduct. This, in turn, clamps the voltage spike across the rectifier diode. At this stage, the active clamp switch, S_c, is turned off and the energy stored in leakage inductor (L_K) discharges the output capacitances of S_2 and S_3. The primary side voltage decreases to zero and the body diodes of S_3 and S_4 begin to conduct. This stage ends when the current decreases to $i_p(t_1)$.

$$\frac{di_{LK}(t)}{dt} = \frac{1}{L_k}\left[\frac{3V_0}{2n} - \frac{V_{in}}{n^2}\right] \quad \text{..... (8)}$$

2.4 Mode 4 (t_3–t_4)

At t_3, diode D_c is cut off and V_{rec} keeps at $\frac{V_{in}}{n}$. The voltage spike across the rectifier is reduced. The circulating current (i.e., is the sum of input current and reflected output current) decreases to zero. The ideal output voltage (V_0) and ideal clamp capacitor voltage are determined by

$$V_{o(ideal)} = \frac{nV_{in}}{2(1-D)} \quad \text{..... (9)}$$

$$V_{c(ideal)} = \frac{V_{in}}{2(1-D)} \quad \text{..... (10)}$$

2.5 Mode 5 (t_4~t_5)

At t_5, S_1 turns off. The intrinsic capacitors of S_1 and S_2 are charged with reflecting load current. When voltage across S_1 reaches to V_{in}, the body diode of S_2 gets conducted. Thus, S_2 can achieve ZVS on. The voltage transition mode of lagging leg switches is similar to that of the conventional PSFB converter. Furthermore, the voltage increases very fast because of large primary current reflected from the load current. When the body diode of S_2 conducts, the voltage across the primary winding is clamped to zero. At the same time the current through diode D_1 is

$$I_{D1} = n(i_{LK} - i_m) \quad \text{..... (11)}$$

After i_{Lk} becomes smaller than i_m, the current of the secondary side of the transformer flows in the reverse direction through the junction capacitors of D_1 and D_2. When the voltage across D_1 is increased to V_{01}, I_{D2} similarly flows through the junction capacitor of D_2. So V_{D2} is decreased to V_{02}.

2.6 Mode 6 (t_5–t_6)

Since both D_1 and D_2 are in the off state, the secondary side of the transformer is regarded as open circuit during mode 6. Thus, only a small magnetizing current flow in reverse direction through the primary side of the transformer, contributing low circulating energy

After t_6, the other half switching cycle begins. Owing to the symmetry operation characteristic, the principles and the equivalent circuits of the other half switching cycle are same as those mentioned earlier.

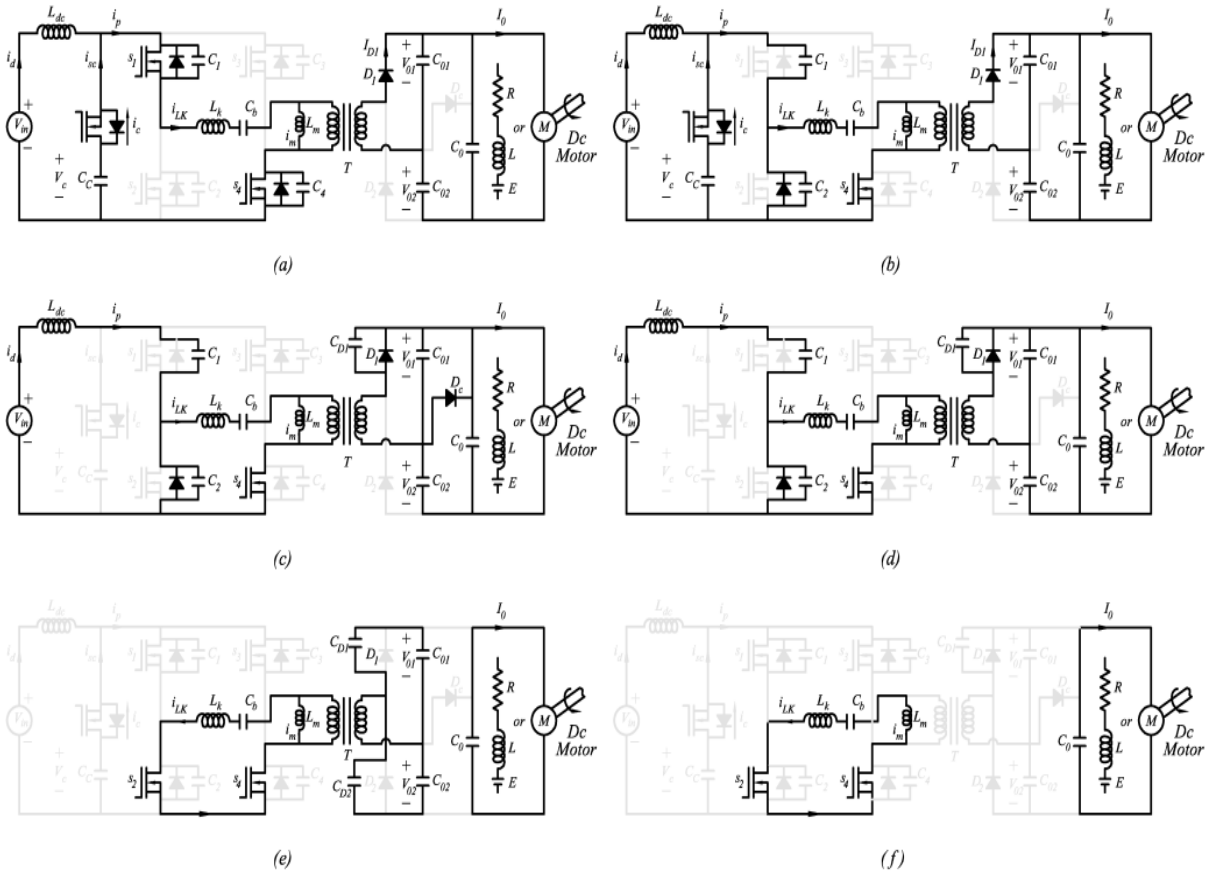

Fig. 3. Equivalent circuits: (a) mode 1, (b) mode 2, (c) mode 3, (d) mode 4, (e) mode 5, (f) mode 6

3. DESIGN CONSIDERATIONS

In this section, the proposed converter design procedure is illustrated by using a prototype converter with the specifications that the input voltage V_{in} is 60 V, switching frequency(F_s) is 60 kHz, leakage inductance (L_k) is 23 µH, and output voltage is 220 V. The design parameters of the prototype converter are given in Table 1.

3.1 Selection of Resonant Frequency

To reduce the current stresses of rectifier diodes and conduction losses, the resonant frequency (F_r), which is determined by the leakage inductance and the rectifier capacitance, should be lower than the switching frequency (F_s). Resonant frequency is determined by using rectifier capacitance and leakage inductance. Rectifier capacitance can be calculated by using the following equation:

$$C_{01} = C_{02} = \frac{n^2}{8\pi^2 L_k F_s^2}\left[\frac{F_s}{F_r}\right]^2 \qquad \text{..... (12)}$$

Fig.4 shows the selection of resonant frequency. Owing to the capacitive output filter, the average value of diode current (I_{D1}) is same as that of the load current in each case. From Fig 4, the waveforms of the current can be represented in (i) triangular form, (ii) sinusoidal form, and (iii) quasi-sinusoidal form. When the resonant frequency is slower than the switching frequency, the waveforms of the current can be of triangular form, which is represented as a dotted line in Fig 4. As the resonant frequency gets faster (F_r), the waveforms of diode current (I_{D1}) can be similar to a quasi-sinusoidal form.

In addition to this, when F_r becomes faster than F_s, the waveforms of diode current (I_{D1}) can be of sinusoidal form. Because the peak value of the diode current (I_{D1}) is smallest, its form is quasi-sinusoidal. F_r can be properly determined by reducing conduction losses and current stresses. As shown in Fig. 4, the peak value of diode current and the rectifier capacitance(C_{01} (or) C_{02}) are selected according to the normalized frequency F_r/F_s, with conditions such as L_k = 23 µH, I_0 = 2.2 A, and F_s= 60

kHz. The peak value of I_{D1}has the smallest value when F_r/F_s is approximately 0.85.

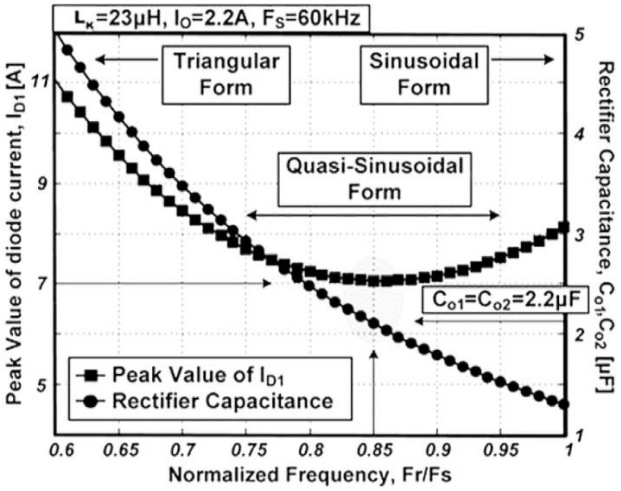

Fig. 4. Selection of resonant frequency

3.2 Selection of the Dead Duty Ratio

To prevent the arm short between both switches in the same leg, the turn-on of each switch in the same leg must be delayed by $D_{dead}T_s$after the turn-off of its opposite switch. Especially, to guarantee safe ZVS operations, the dead time between switches has to be greater than the maximum ZVS time (T_z), which is the required time for the ZVS of the lagging leg under the worst ZVS condition. Therefore, the maximum ZVS time (T_z) can be obtained as follows:

$$T_z = V_{in}\frac{2C_{oss}}{i_p(t)} \qquad \text{.....(13)}$$

Where C_{oss} is the output capacitors of power switches.

3.3 Selection of Turn Ratio of Transformer

Mode 1 of the operation of the converter is to be considered for to derive the DC conversion ratio. During mode 1, the current through the rectifier diode D_1 can be obtained as follows:

$$I_{D1}(t) = \frac{1}{Z_0}\left(\left(\frac{V_{in}}{n} - V_{01}(t)\right)\sin\omega_r(t-t_0)\right) \text{....(14)}$$

From here, the charging current of C_{01} and discharging current of C_{02} flow through D_1. The average value of charging current of C_{01} during (T_s/2) half switching period is equal to that of the load current (I_0). In addition, the bias value of V_{01} is equal to half of the output voltage (V_0/2). According to Kirchhoff's voltage law, the output voltage is equal to the sum of V_{01} and V_{02}. Thus, the variation in V_{01} can be represented as follows:

$$\Delta V_{01} = \frac{1}{C_{01}}\int I_{co1}(t)dt = \frac{1}{C_{01}}\frac{T_s}{2}I_0 \qquad \text{..... (15)}$$

Therefore, $V_{01}(t)$ can be defined as follows:

$$V_{01}(t_0) = \frac{V_0}{2}\left[1 - \frac{T_s}{2C_{01}R_0}\right] \qquad \text{.....(16)}$$

By averaging the current of the rectifier diode I_{D1}, the load current can be derived as follows:

$$I_0 = \frac{V_0}{Z_L} = \frac{1}{T_s\omega_r}\left[\frac{1}{Z_0}\left(\frac{V_{in}}{n} - V_{01}(t_0)\right)\times\left(1-\cos\left(\frac{T_s}{2}\omega_r D_{eff}\right)\right)\right] \qquad \text{..(17)}$$

From Equations (16) and (17), the DC conversion ratio of the overall system can be represented as follows:

$$\frac{V_0}{V_{in}} = \frac{1}{n\left[\frac{Z_0}{Z_L}\left(\frac{2\pi F}{1-\cos(\pi F D_{eff})}\right) + \frac{1}{2}\left(1 - \frac{T_s}{2C_{01}R_0}\right)\right]} \qquad \text{..... (18)}$$

Where D_{eff} is the effective duty ratio. By solving the above equation, we can calculate the turns ratio of the transformer.

3.4 Selection of Leakage Inductance (L_K)

The required leakage inductance (L_k) for ZVS operation is determined by the output power and switch stray capacitors. Leakage inductance L_k must be greater than 100 nH for ZVS operation to occur, but needs to have a higher value to reduce the peak value of circulating current and thus to reduce rms current at the switches and transformer windings. The minimum value of L_k necessary for ZVS to turn on is given by the following equation:

$$L_K \geq \frac{C_{eq}}{2}\left(\frac{V_{in} - nV_0}{i_{Lk}}\right)^2 \qquad \text{..... (19)}$$

4. PERFORMANCE ANALYSIS OF THE PROPOSED DC–DC CONVERTER

4.1 ZVS Condition for the Leading Leg Switches

In the traditional PSFB converter, the ZVS operation of the leading leg switches can be easily achieved due to the large output filter inductor. But the large output inductance causes core loss due to the saturation of the core. This is eliminated with the help of the proposed converter to use the converter

without additional inductance, the leakage inductance of the transformer is utilized as the resonant inductor. The energy stored in the leakage inductor must discharge to the voltage level of zero before the switch is turned on. At that time, body diode of switch starts conducting and the switch current increases. Now the switch attains ZVS turn on. To ensure ZVS the energy stored in the leakage inductor must be greater than that stored in the switch. The minimum value of current required for ZVS can be represented as follows:

$$I_0^{ZVS} = n^2 V_H \sqrt{\frac{C_{eq}}{L_K}} \quad \text{..... (20)}$$

Where V_H is the threshold voltage.

The dead gap between the auxiliary switch gating signal and main switch gating signal can be obtained as follows:

$$t_{Dc} = \pi \frac{\sqrt{2L_K C_{eq}}}{n} \quad \text{..... (21)}$$

4.2 Reduction of Circulating Current

The conventional PSFB converter has a drawback due to the phase-shifted PWM control, that is, the circulating current flowing through transformers and switching devices during the freewheeling interval. This circulating current is the sum of reflected load current and transformer primary magnetizing current, which increases the conduction loss and RMS current stresses of components. However, the active clamping switch, leakage inductor of the transformer, and clamping diode can reduce this circulating current.

4.3 Reduction of Current Stress and Conduction Losses by Using Resonance

Usually, the voltage doubler causes voltage–current doubling effect, which creates current stresses across the rectifier diodes. But the proposed converter eliminates this with the help of resonance between the leakage inductance of the transformer and rectifier capacitors.

4.4 Reduction of Voltage Stress of the Rectifier Diode

Owing to the clamp diode, D_C, the voltage stress across the rectifier diodes is reduced to $3V_0/2$. To show the improvement of the converter in reducing voltage stress, a prototype with low input and high output voltage is designed. The input is 45–60 V and the output is 220 V. Considering the duty cycle loss caused by the leakage inductance, the turn ratio of the transformer in prototype is higher than that of the ideal calculation. From Table 2 it can be seen that the voltage stress in the proposed converter is minimized. Thus, the diode with lower breakdown voltage can be used to reduce the conduction loss and reverse the recovery loss.

4.5 Reduction of Filter Requirements

In the proposed converter, the energy stored in the leakage inductance is transferred to the output side during the freewheeling period, so the requirement of the output filter inductor is reduced. The current ripple (peak to peak) is derived in Equation (22) according to different duty cycle.

$$I_{pp} = \frac{V_0}{4L_K}(1-D)T_s \quad \text{..... (22)}$$

The current ripple in function of input V_{in} is derived as:

$$I_{pp} = \frac{V_0(V_{in} - nV_0)}{2L_K(2V_{in} - nV_0)} T_s \quad \text{.....(23)}$$

The ripple reduction in the proposed converter is approximately 80%–90% during the input voltage range compared with that in the conventional PSFB.

5. SIMULATION RESULTS

The proposed converter has been simulated for given specifications in Table 1 by using MATLAB Simulink software for input voltage (V_{in}) = 60 V, output voltage (V_o) = 220 V, and power = 1.5 kW. Simulation results are illustrated in Fig. 5. Voltage across the primary side of the transformer and its current is depicted in Fig. 5a. From the waveform, it is clear that there is no circulating current in the primary side of the transformer. Soft-switching operation of the proposed converter is depicted in Fig. 5b and it is clear that the voltage across the switch naturally clamps to zero and then corresponding antiparallel body diode starts conducting before the switch is turned on, which ensures ZVS turn-on. Output voltage waveform is shown in Fig. 5d. From the waveform, the output filter requirement of the proposed converter is low compared to that of the conventional PSFB converter.

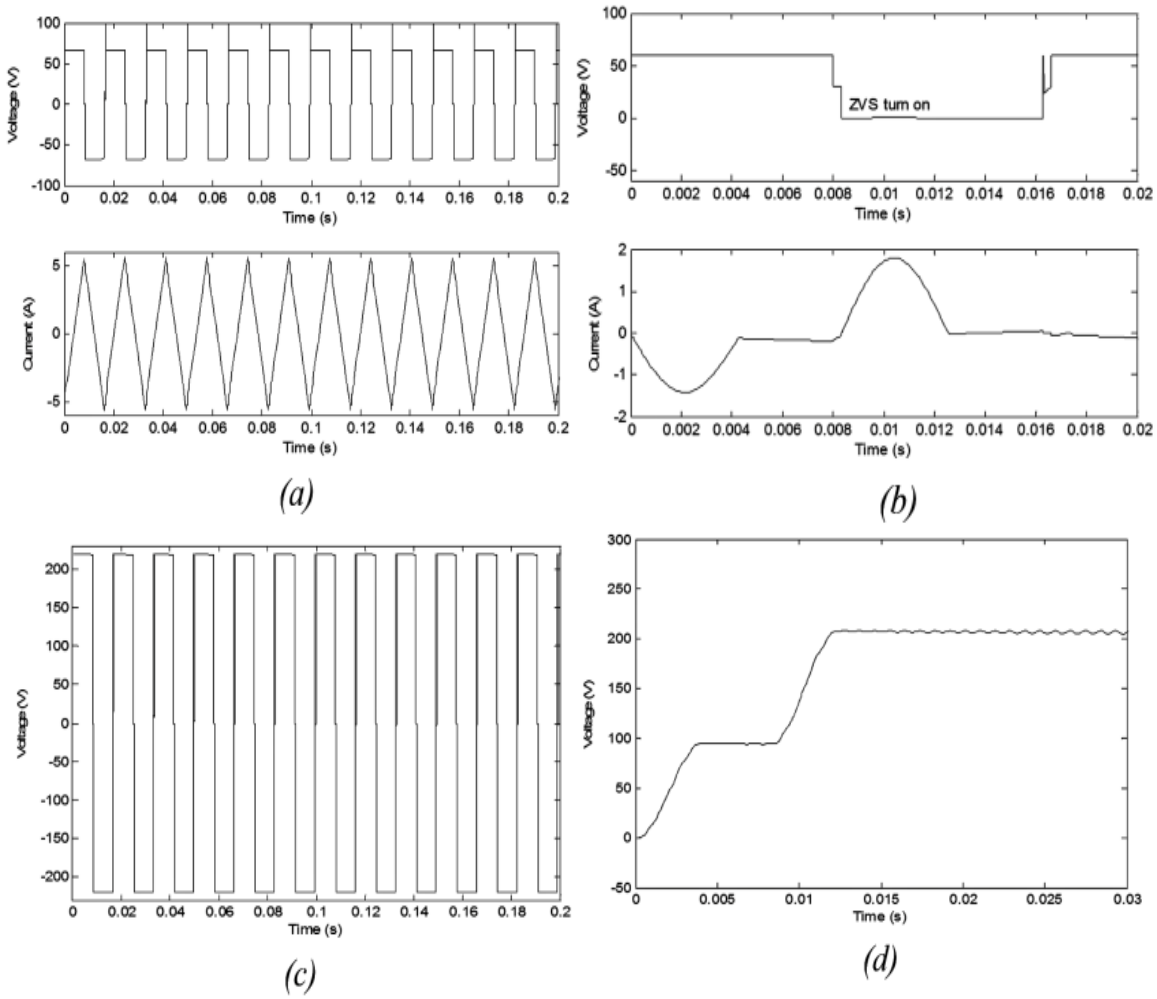

Fig. 5. Simulated waveforms of the proposed converter: (a) primary voltage and primary current of the transformer, (b) ZVS turn on and its current, (c) secondary voltage of the transformer, (d) output voltage of the proposed converter

6. EXPERIMENTAL INVESTIGATION

A 1.5 kW prototype of the proposed converter was built to the designed specifications as per Table 1. Experimental results matched closely with simulated waveforms. As explained earlier, due to the lack of output inductor, the voltage stress across the rectifier is highly reduced, facilitating high voltage without ringing. In addition, because all stored energy in the transformer leakage inductance is transferred to the output side simultaneously during powering and freewheeling mode, circulating energy is reduced, eliminating the circulating loss. So during the freewheeling period, only a small magnetizing current flows through the primary side of the transformer. The resonance between the transformer leakage inductance and rectifier capacitor reduces the current stress, voltage spike of the rectifier diodes, and conduction losses. The experimental setup is shown in Fig.6.

Soft- switching operation at different load conditions with input voltages 60 and 100 V is depicted in Figs. 7 and 8, respectively. From the waveform, it is confirmed that all switches in the proposed converter are turned on with ZVS under entire load condition while having no effect of circulating current and voltage stress. Figs. 9a and 9b show the gate signal and drain to source voltage of main switch as well as an auxiliary clamp switch. From the measured waveform, it is confirmed that the drain-to-source voltage reaches zero before the gate signal reaches its threshold voltage. Therefore, the ZVS operation of main switch as well as an auxiliary clamp switch is well achieved. Fig 9d shows the voltage and current waveform on the primary side of the transformer. From the measured waveform, it is confirmed that the circulating current is well reduced in the proposed converter

To calculate the efficiency of the proposed converter, the amount of losses should be taken into consideration.

Efficiency = output/(output + losses). The main losses in the converter are conduction loss, switching loss, and inductor loss.

$$P_{\text{loss}} \cong Ps_1, s_4(switching) + Ps_1, s_4(conduction) + Ps_2, s_3(switching) + Ps_2, s_3(conduction) + P_{D_1}, {}_{D_2}, {}_{D_c}(switching) + P_{D_1}, {}_{D_2}, {}_{D_c}(conduction) + P(inductor\ loss) \quad \ldots\ldots\ldots\ldots (24)$$

In the proposed converter, switching loss is eliminated because of the soft-switching operation. Inductor used is also very small, so induction loss is also negligible. By using the clamping diode, the voltage stress across the rectifier is mostly eliminated, so the conduction loss is also small. Owing to the elimination of switching losses and inductor losses, efficiency is higher compared to that reported in reference [11].

The efficiencies of the prototype are evaluated and shown in Fig. 10. The proposed converter has maximum efficiency of 98.87% at full load and achieves a significant improvement in the efficiency compared with the in article [11], as the proposed converter operates with ZVS under entire load conditions while having no effect of duty-cycle loss, circulating current, and turn-off switching losses, as shown in the waveforms. The elimination of the secondary-voltage overshoot, its oscillation, and use of a low-voltage-rated diode can help in improving the efficiency.

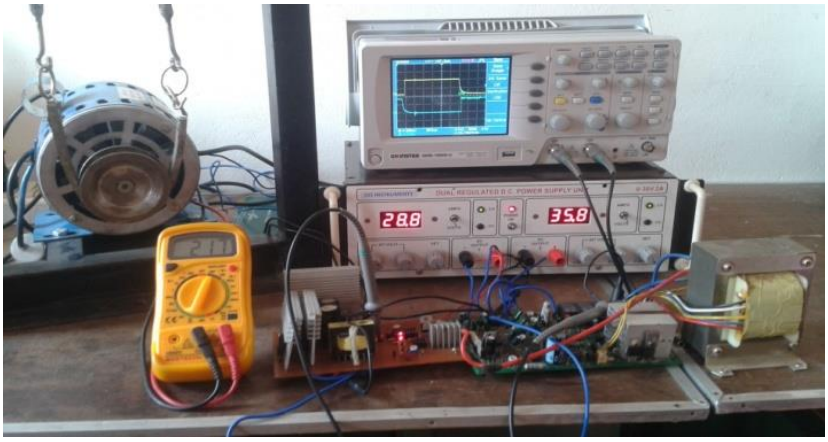

Fig. 6. Experimental setup of the proposed converter

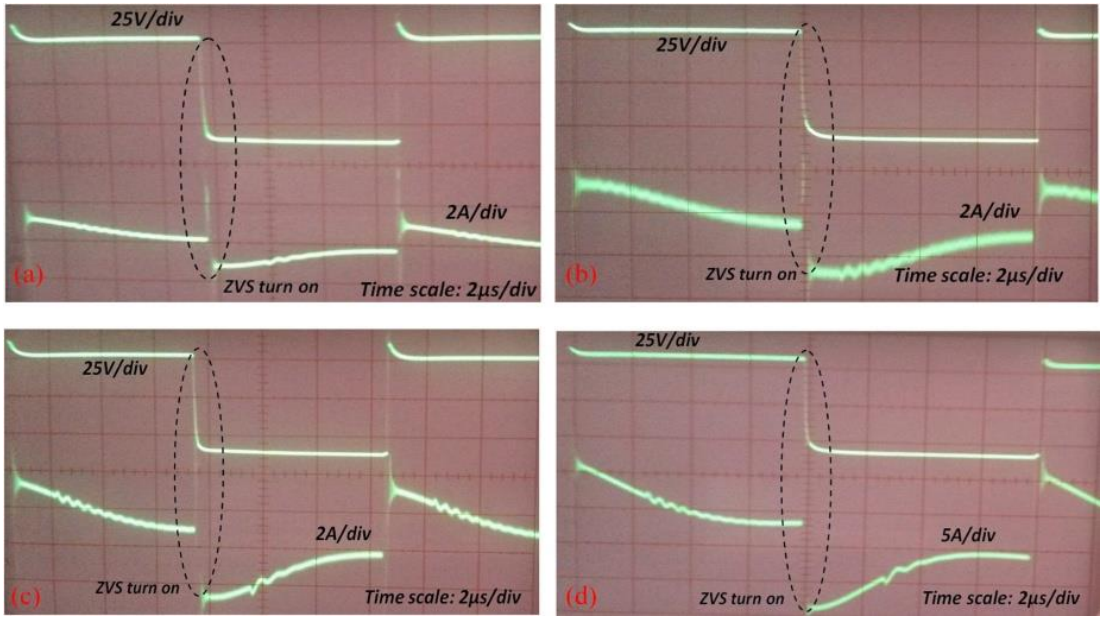

Fig. 7. Experimental waveforms of soft switching operation on different load condition input V_{in} = 60 V at(a) no load, (b) 25% load, (c) 80% load, and (d) full load conditions

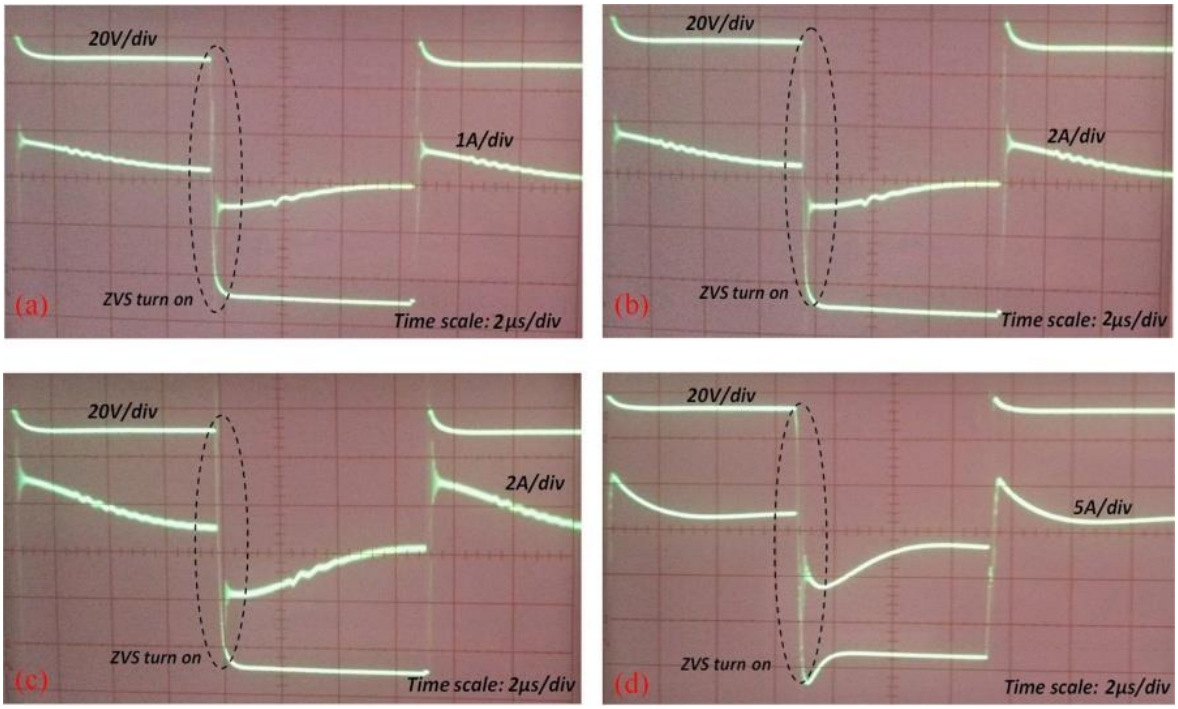

Fig. 8. Experimental waveforms of soft switching operation on different load condition input V_{in} =100 V, at(a) no load, (b) 25% load, (c) 80% load, and (d) full load conditions

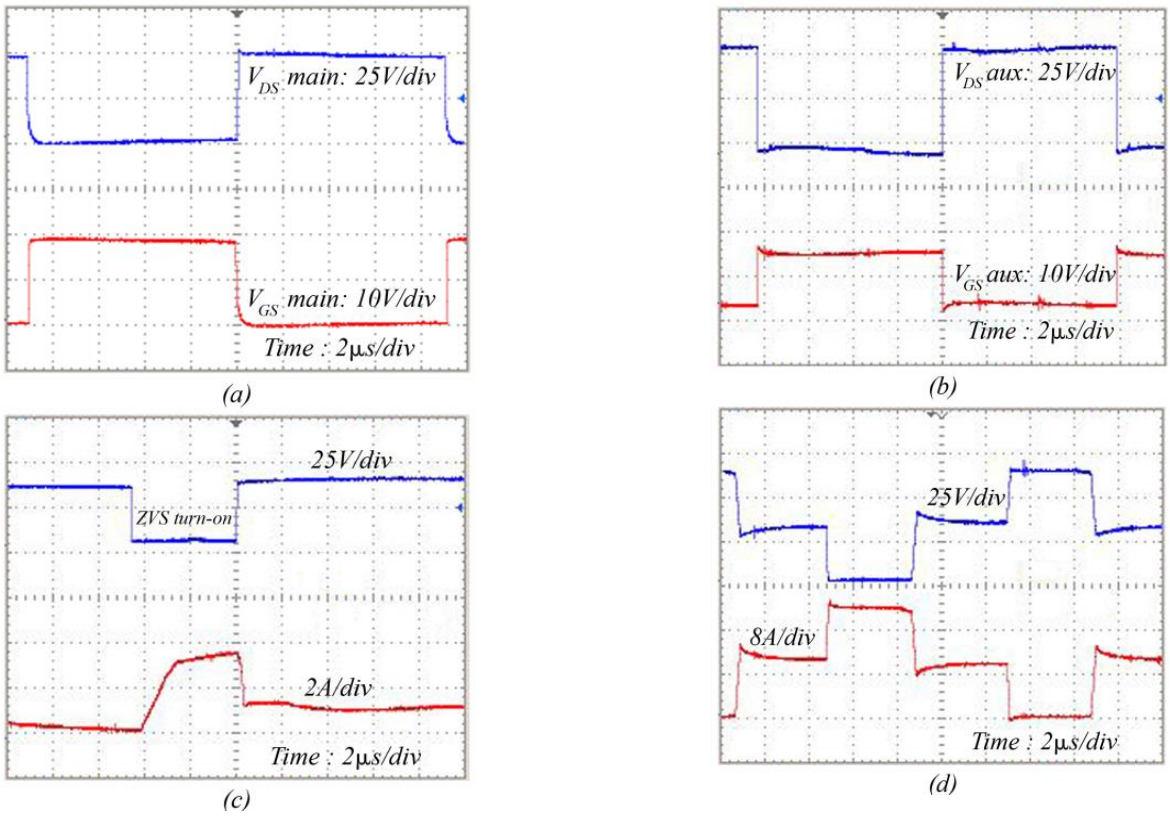

Fig. 9. Experimental waveforms of (a) main switch voltage and gate voltage, (b) auxiliary switch voltage and gate voltage, (c) ZVS turn on and its current, (d) primary voltage and primary current of the transformer

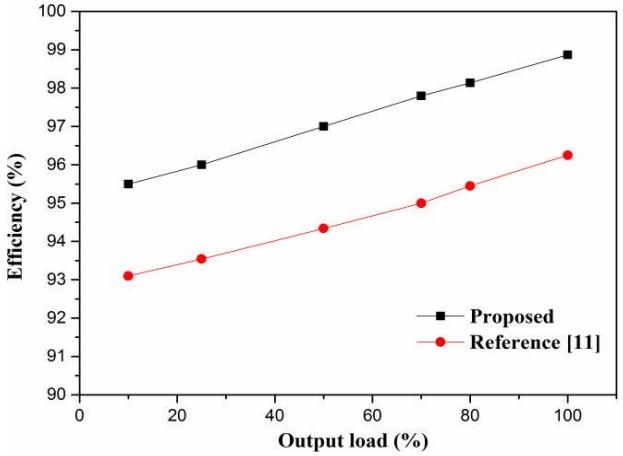

Fig. 10. Determination of efficiency

Table 1: Parameters of the prototype circuit

Item	**Symbol**	**Value /Part**
Input voltage	V_{in}	60 V
Max. power rating	P_{max}	1.5 kW
Switching frequency	F_s	60 kHz
Transformer	4:30/EE42	4:30/EE42
Leakage inductance	L_k	23 µH
Magnetizing inductance	L_m	30 µH
Capacitance of double cell	C_{01}, C_{02}	2.2 µF
Output capacitance	C_0	1000 µF
Power switches	$S_{1\text{-}4}$, S_c	FA57SA50LC
Rectifier diodes	$D_{1\text{-}2}$, D_c	DSEK60-06 A
Clamping capacitor	C_c	3 µF
Boost inductor	L_{dc}	33 µH
Output voltage	V_0	220 V
DC machine	1)	0.5 HP, 220 V

Table 2: Voltage stress across the secondary side using different reset circuits

S. No.	Topology	V_{recmax} equation	V_{recmax} for the prototype V_0 = 220 V, V_{in} = 60 V, $n = 4/30$
1.	[10]	$2\frac{V_{in}}{n} - V_0$	$2\frac{V_{in\,max}}{n} - 220 = 680$ V
2	[11]	$\frac{V_{in}}{n} + V_0$	$\frac{V_{in}}{n} + V_0 = 670$ V
3	[12]	$2\frac{V_{in}}{n} - \frac{V_0}{2}$	$2\frac{V_{in}}{n} - \frac{V_0}{2} = 790$ V
4	[13]	$2\frac{V_{in}}{n}$	$2\frac{V_{in}}{n} = 900$ V
5	[14]	$2\frac{V_{in}}{n} - \frac{V_0}{2}$	$2\frac{V_{in}}{n} - \frac{V_0}{2} = 790$ V
6	Proposed	$3V_0/2$	$3V_0/2 = 330$ V

7. CONCLUSION

A new active clamped current fed full-bridge DC–DC converter is presented. By using a single active clamp circuit and a clamp diode, the voltage stress across the rectifier is reduced, and low-voltage-rated diode can be used to reduce the conduction losses. In addition, since all energy that is stored in the leakage inductor of the transformer is transferred to the output side, the circulating energy is considerably reduced. A prototype verifies the theoretical analysis, and the efficiency is found to be improved more than 3% at full load. Owing to the advantages, the proposed converter is applicable especially for the high voltage application such as speed and torque control of DC motors, plasma display panel sustain power module, and high-voltage battery charger.

REFERENCES

[1] D. Gautama, F. Musavi, M. Edington, W. Eberle, and W. G. Dunford, *"An automotive on—board 3.3 kW battery charger for PHEV application,"* Proc. IEEE Vehicle Power Propulsion Conf., pp. 1–6, Sep. 2011.

[2] P. K. Jain, W. Kang, H. Soin, and Y. Xi, *"Analysis and design considerations of a load and line independent zero voltage switching full bridge dc/dc converter topology,"* IEEE Trans. Power Electron., Vol. 17, no.5, pp. 649–657, Sep. 2002.

[3] X. Wu, J. Zhang, X. Xie, and Z. Qian, *"Analysis and optimal design considerations for an improved full bridge ZVS dc–dc converter with high efficiency,"* IEEE Trans. Power Electron., Vol. 21, no. 5, pp.1225–1233, Sep. 2006.

[4] L. H. Mweene, C. A. Wright, and M.F. Schlecht, *"A 1 kW 500 kHz front-end converter for a distributed power supply*

system," IEEE Trans. Power Electron., Vol. 6, no. 3, pp. 398–407, July 1991.

[5] W. Li, Y. Shen, Y. Deng, and X. He, *"Interleaved converter with voltage multiplier cell for high set-up and high-efficiency conversion,"* IEEE Trans. Power Electron., Vol. 25, no. 9, pp. 2397–2408, Sep. 2010.

[6] Y. Zhao, W. Li, Y. Deng, and X. He, *"Analysis, design and experimentation of an isolated ZVT boost converter with coupled inductors,"* IEEE Trans. Power Electron., Vol. 26, no. 2, pp. 541–550, Feb. 2011.

[7] W. Li, W. Li, and X. He, *"Zero-voltage transition interleaved high step-up converter with built-in-transformer,"* IET Power Electron., Vol. 4, no. 5, pp. 523–531, May 2011.

[8] W. Li, Y. Zhao, J. Wu, and X. He, *"Interleaved high step-up converter with winding-cross-coupled inductors and voltage multiplier cells,"* IEEE Trans. Power Electron., Vol. 27, no. 11, pp. 133–143, Jan. 2012

[9] H. Bodur, and A. F Bakan, *"A new ZVT-ZCT-PWM DC–DC converter,"* IEEE Trans, Power Electron., Vol. 19, no. 3, pp. 676–684, May 2004.

[10] W.-J. Le and G.-W. Moon, *"A new phase-shifted full-bridge converter with voltage-doubles-type rectifier for high-efficiency PDP sustaining power module,"* IEEE Trans. Ind. Electron., Vol. 55, no. 6, pp. 2450–2458, June 2008.

[11] I.-O. Lee and G.-W. Moon, *"Phase-shifted PWM converter with a wide ZVS range and reduced circulating current,"* IEEE Trans. Power Electron., Vol. 28, no. 2, pp. 908–919, Feb. 2013.

[12] J.-H. Lee, D.-H.Yu, J.-G.Kim, Y.-H.Kim, S.-C.Shin and D.-Y.Jung, *"Auxiliary switch control of a bidirectional soft-switching DC/DC converter,"* IEEE Trans. Power Electron., Vol. 28, no.1 2, pp. 5446–5457, Dec. 2013.

[13] I.-O. Lee and G.-W. Moo, *"Soft-switching DC/DC converter with a full ZVS range and reduced output filter for high-voltage applications,"* IEEE Trans. Power Electron., Vol. 28, no. 1, pp. 112–122, Jan. 2013.

[14] N. Altintas, A. F. Bakan, and I. Aksoy*"A novel ZVT-ZCT-PWM boost converter,"* IEEE Trans. Power Electron., Vol. 29, no. 1, pp. 256–265, Jan. 2014.

[15] T.F. Wu, Y.-C.Chen, J.-G.Yang and C.-L.Kuo, *"Isolated bidirectional full-fridge DC–DC converter with a fly back snubber,"* IEEE Trans. Power Electron, Vol. 25, no. 7, pp. 1915–1922, July 2010.

[16] A. Mousavi, P. Das, and G. Moschopoulos, *"A comparative study of a new ZCS DC–DC full-bridge boost converter with a ZVS active-clamp converter,"* IEEE Trans. Power Electron,Vol. 27, no.3, pp.1347–1358, Mar. 2012.

[17] I.-O. Lee and G.-W. Moon, *"The k-Q analysis for an LLC series resonant converter,"IEEE Trans. Power Electron*, Vol. 29, no. 1, pp. 13–16, Jan. 2014.

[18] E. H. Kim, and B.-H. Kwon, *"Zero voltage and zero current switching full-bridge converter with secondary resonance,"* IEEE Trans. Ind. Electron., Vol. 57, no. 3, pp. 1017–1025, Mar. 2010.

[19] U. K. Madawala, M. Neath, and D. J. Thrimawithana, *"A power-frequency controller for bidirectional inductive power transfer systems,"*IEEETrans. Ind. Electron., Vol. 60, no. 1, pp. 310–317, Jan. 2013.

[20] J. C. Crebier, B. Revol, J. P. Ferrieux, *"Boost-chopper-derived PFC rectifiers interests and reality,"* IEEE Trans. Ind. Electron.,Vol. 52, no. 1, pp. 36–45, Feb. 2005.

[21] W. Li, and X. He, *"Zero-voltage transition interleaved high step-up converter with built-in-transformer,"*IET Power Electron.,Vol. 4, no. 5, pp. 523–531, May 2011.

[22] W. Yu, J. S. Lai, W.H. Lai, H. Wan, *"Hybrid resonant and PWM converter with high efficiency and full soft-switching range,"* IEEE Trans. Power Electron., Vol. 27, no. 12, pp. 4925–4933, Dec. 2012.

[23] H. J. Chiu, and L. W. Lin, *" A high-efficiency soft-switched AC/DC converter with current-doubler synchronous rectification,"*IEEE Trans. Power Electron, Vol. 52, no. 3, pp. 709–718, Jun. 2005.

[24] J. Y. Lee, *"An improved magnetic-coupled AC–PDP sustain drive with dual recovery paths,"* IEEE Trans. Ind.Electron., Vol. 54, no. 3, pp. 1623–1631, Jun. 2007.

[25] B. GU, J.S. Lai, N. Kees, and C. Zheng, *"Hybrid switching full bridge DC–DC converter with minimal voltage stress of bridge rectifier, reduced circulating losses, and filter requirement for electric vehicle battery chargers,"*IEEE Trans. Power Electron., Vol. 28, no. 3, pp. 1132–1144, Mar. 2013.

[26] Y. Lembeye, V.D. Bang, G. Lefevre, J.P. Ferrieux, *"Novel half-bridge inductive dc–dc isolated converters for fuel cell applications,"* IEEE Trans. Energy Convers., Vol. 24, no.1, pp. 203–210 Mar. 2009.

[27]. V. Yakushev, V. Meleshim, S. Fraidlin, *"Full bridge isolated current fed converter with active-clamp,"*Proc. IEEE Power Electron. Spec. Conf. Expo. pp. 560-566, 1999.

[28]. M. Nymand, M.A. e. Andersen, *"High- efficiency isolated boost dc–dc converter for high- power low-voltage fuel cell applications,"* IEEE Trans. Ind. Electron., Vol. 57, pp. 505–514, 2010.

[29] P. Das, B. Laan, S.A. Mousavi, G. Moschopoulos, *"A non-isolated bidirectional ZVS-PWM active clamped dc–dc converter,"*IEEE Trans. Power Electron., Vol. 24, no. 2, pp. 553–558, Feb. 2009.

[30] W. Song, B. Lehman, *"Current-fed dual-bridge dc–dc converter,"*IEEE Trans. Power Electron., Vol. 22, no. 2, pp. 461–469, Mar. 2007.

[31] W. Li, S. Zong, F. Liu, B. Wu, *"Secondary-side phase-shift-controlled ZVS DC/DC converter with wide voltage gain for high input voltage applications,"*IEEE Trans. Power Electron., Vol. 28, no. 11, pp. 5128–5139, Nov. 2009.

[32] U.R. Prasanna, A.K. Rathore, *"Analysis, design and experimental results of a novel soft-switching snubberless current-fed half bridge front-end converter,"* IEEE Trans. Power Electron., Vol. 28, no. 1, pp. 3219–3230, July 2013.

[33] P. Xuewei, A.K. Rathore, *"Novel bidirectional snubberless naturally commutated soft-switching current-fed full-bridge isolated DC/DC converter for fuel cell vehicles," I*EEE Trans. Ind. Electron., Vol. 61, no.5, pp. 2307–2315, May 2014.